A 10 kW high-voltage pulse generator for corona plasma generation

A 10 kW high-voltage pulse generator for corona plasma generation

K. Yan,[a] E. J. M. van Heesch, A. J. M. Pemen, P. A. H. J. Huijbrechts, and Piet C. T. van der Laan
EVT Group, Faculty of Electrical Engineering, Eindhoven University of Technology, 5600 MB Eindhoven, The Netherlands

(Received 3 October 2000; accepted for publication 22 February 2001)

In this article we discuss a 10 kW high-voltage pulse generator for producing corona-induced plasma. The generator mainly consists of a three-step resonant charging circuit switched by thyristors, a transmission line transformer, and a triggered spark-gap switch. Voltage pulses of 30–100 kV with a rise time of about 20 ns, a pulse duration of 50–250 ns, pulse repetition rate of 1–900 pulses per second, energy of up to 12 J/pulse, and an average power of up to 10 kW have been achieved with a total energy transfer efficiency of about 80%–90%. At each frequency, the deviation of the energy per pulse is around 1.0%. Moreover, the generator has been tested for more than 100 h for both industrial demonstrations and laboratory investigations at an average output power of 1–10 kW. © *2001 American Institute of Physics.* [DOI: 10.1063/1.1367358]

I. INTRODUCTION

Worldwide research and development on corona plasma techniques for pollution control and sustainable development are gradually leading to industrial applications. Investigations range from odor treatment, indoor air cleaning, volatile organic compound (VOCs) abatement, and flue gas cleaning to CO_2 conversion and biogas cleaning.[1–3] To successfully promote these industrial applications, the availability of highly efficient and reliable high-voltage-pulsed power sources is critical. In previous work,[2,4] we have reported that by using various voltage pulses and/or corona reactors pulsed streamer coronas may develop into two phases, corresponding to primary and secondary streamers. Energy transfer during these two phases depends on the voltage rise rate and the pulse duration. Optimized relationships among the voltage rise time, the peak voltage, the pulse duration, the size of corona reactor, the output impedance of the high-voltage pulse generator, the stray capacitance of the corona reactor, and the corona energy transfer per unit length of reactor are also discussed.[3–5] Most critical elements of the corona-induced plasma system, such as high-voltage switching, transmission line transformer, electrical diagnostics, and costs of the voltage pulse generator are discussed in separate papers.[6,7] A general principle for designing a corona plasma system has been proposed in order to improve the initial radical production and to increase the total energy transfer efficiency.[7] According to the proposed design principle, in this article we discuss a 10 kW repetitive high-voltage pulse generator. The ultimate objective of this work is to develop an industrial corona-induced plasma system with an average power of 50–100 kW. Characteristics of corona plasma in a wire-plate reactor, the triggered spark-gap switching, and the spark-gap lifetime evaluation will be reported in separate papers.

[a]Electronic mail: k.yan@tue.nl

II. VOLTAGE PULSE GENERATOR

A. Main electrical circuit

Figure 1 shows a schematic diagram of the electrical circuit with a resistor as load. The pulse transformer separates the low- and high-voltage parts of the circuit.[6] The low-voltage part consists of a main filter, a set of rectifiers, a three-step resonant charging circuit that is switched by thyristors, and the primary winding of the pulse transformer TR. The high-voltage part consists of the secondary winding of the pulse transformer TR, a high-voltage diode D, an air coil inductor L_3, a high-voltage energy storage capacitor C_h, a triggered spark-gap switch S, a transmission line transformer (TLT), and Metglas magnetic cores placed around the TLT cables. The TLT is constructed with four 50 Ω coaxial cables (RG218). At the input side, four cables are connected in parallel ($Z_{in}=12.5\,\Omega$). At the output side, four cables are divided into two sets, and in each set the two cables are connected in parallel. Then, the two sets are connected in series ($Z_{out}=50\,\Omega$). All four cables can be also connected in series, which gives output impedance of 200 Ω.[6] All electrical parts including the TLT are operated in air. The TLT and the Metglas cores are specially designed in order to limit energy losses by the secondary mode current and to minimize their effect on the voltage rise time and the voltage gain.

In order to stabilize the switching voltage of the spark-gap switch and the output energy per pulse, the three thyristors, T_1, T_2, and T_3, are switched in series. Detailed discussions of this are given in Refs. 6 and 8. A four-step process generates the voltage pulse. In the first step, the low-voltage capacitor, C_L, is resonantly charged via energy storage capacitor C_0, thyristor T_1 and inductor L_1. During the second step, the high-voltage capacitor C_h is resonantly charged in about 20–70 μs via C_L, L_2, TR, T_2, D, and L_3. Then the stored energy is transferred to the load via a spark-gap switch S and a TLT. Before low-voltage capacitor C_L is charged again, the third thyristor, T_3, is used to correct the voltage

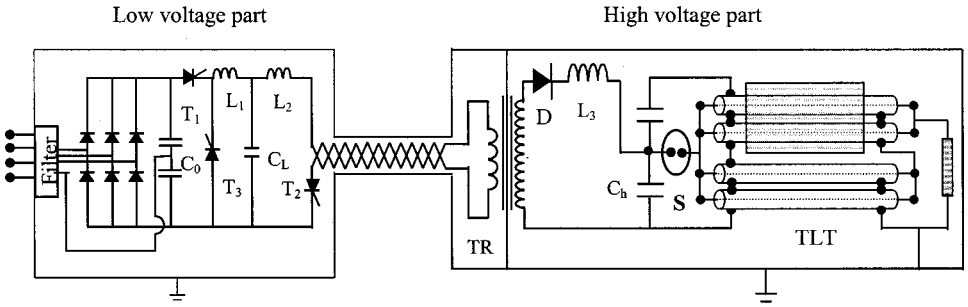

FIG. 1. Schematic diagram of the high-voltage pulsed power generator.

polarity on C_L via T_3 and L_1. Detailed discussions on the spark-gap switch are presented in Sec. II B. The switching voltage of the spark-gap switch and the voltage gain of the TLT determine the output peak voltage.[6] After the main spark gap breaks down, the voltage on capacitor C_h decreases with a time constant of $Z_{\text{in}}C_h$. The generator can produce 30–100 kV peak voltage in a rise time of about 20 ns and pulse duration of 50 to 250 ns.

B. Spark-gap switch and the trigger method

The switch for high voltage and large current may be the most critical element in the development of pulsed power techniques. The properties of the switch significantly affect the cost, efficiency, reliability, and capacity of the generator. Although spark-gap switches have been widely used for pulsed power generation, there is not much in the literature in relation to high repetition rate and long lifetime continuous operation.[9] A newly designed spark-gap switch, shown in Fig. 2, including an inductor L, a capacitor C, and a resistor R formed (LCR) triggering method has been developed to bridge the gap for industrial applications. The arrows indicate the gas flow. Both the main electrode gap and the trigger electrode gap are flushed by a forced gas flow. The gas flows into the spark-gap switch around the trigger electrode, and then flows out via six symmetrical exits under atmospheric pressure. In terms of the pulse repetition rate and the flush gas flow rate, the triggered spark-gap switch may run in a prefiring or a normal switching mode.[9]

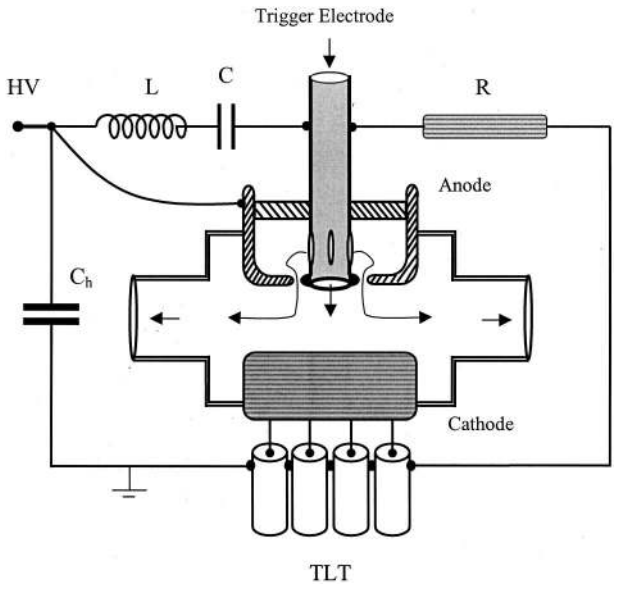

FIG. 2. Newly designed spark-gap switch and the LCR trigger circuit.

The inductor L, capacitor C, and resistor R form the LCR triggering circuit, where we always have $R \gg 2\sqrt{L/C}$ and $C_h \gg C$. After the thyristor T_2 is switched on, the voltage on the high-voltage capacitor C_h will rise as

$$V(t) = \frac{V_{\max}}{2}[1 - \cos(\omega t)],$$

where

$$\omega = \sqrt{\frac{C_L + n^2 C_h}{n^2 C_h C_L \left(L_2 + \frac{L_3}{n^2} \right)}}$$

is the resonant frequency determined by C_L, L_2, TR, L_3, and C_h, and $V_{\max}$ is the maximum voltage on the high-voltage capacitor after resonant charging. The turns ratio of the pulse transformer TR is n. The voltage on the trigger electrode rises as

$$V_T(t) = \frac{V_{\max}}{2} \frac{\omega^2 \tau^2}{1 + \omega^2 \tau^2} \left[\exp\left(-\frac{t}{\tau} \right) - \cos(\omega / t) \right] + \frac{V_{\max}}{2} \frac{\omega \tau}{1 + \omega^2 \tau^2} \sin(\omega t),$$

where $\tau = RC$ and $\omega t \leqslant \pi$. At the end of the charging cycle $\omega t = \pi$, the ratio of the voltage V_T on the trigger electrode to that on the high-voltage capacitor C_h can be expressed approximately as

$$\frac{V_T}{V_{\max}} = \frac{1}{2} \frac{\beta^2}{1 + \beta^2} \left[1 + \exp\left(-\frac{\pi}{\beta} \right) \right],$$

where $\beta = \omega \tau$, which is defined as the time coefficient. After resonant charging of C_h, the smaller capacitor C will be further charged via the LCR circuit by high-voltage capacitor C_h. During this process, the voltage on the trigger electrode decreases exponentially with the time constant τ. The voltage between the anode and the trigger electrode increases exponentially until the trigger gap breaks down. After that, a high frequency current through inductor L and capacitor C brings more energy into the trigger gap. As a result, the main gap is fired also. In order to prevent early firing during the charging period, the voltage ratio $V_T / V_{\max}$ should be carefully designed. Figure 3 shows the dependence of the voltage ratio on the time coefficient β. During our tests, β values in the

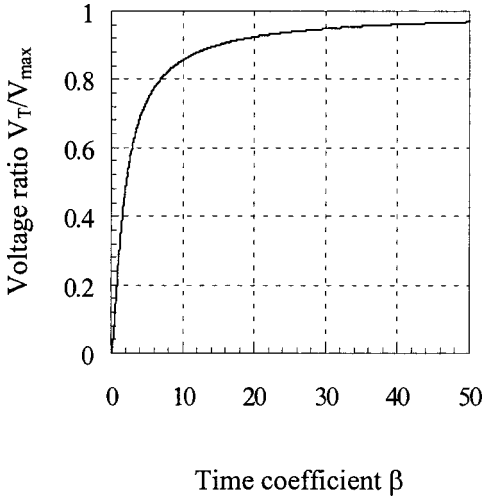

FIG. 3. Dependence of the voltage ratio on the time coefficient.

range of 10–20 give better performance. To avoid prefiring and misfiring, the average electric field in the main gap is designed to be around 26–33 kV/cm in air.[9]

III. RESULTS AND DISCUSSIONS

A. Characteristics of the triggered spark-gap switching

In order to demonstrate the switching behavior of the spark-gap switch, Fig. 4 shows a typical voltage wave form appearing on high-voltage capacitor C_h after switch on of thyristor T_2. The voltage first increases during the resonant charging process, and then remains almost constant until the main spark gap is fired. The delay between the end of the charging cycle and closure of the spark-gap switch mainly depends on the time coefficient β and the voltage pulse repetition rate [pulses per second (PPS)]. Figure 5(a) shows an averaged time-resolved voltage wave form based on 12 signals. Each fast voltage drop corresponds to one of the moments that the main spark gap breaks down. The time derivative of the averaged voltage obviously demonstrates the switching behavior, indicated in Fig. 5(b). The positive part corresponds to the charging current, while the negative peaks

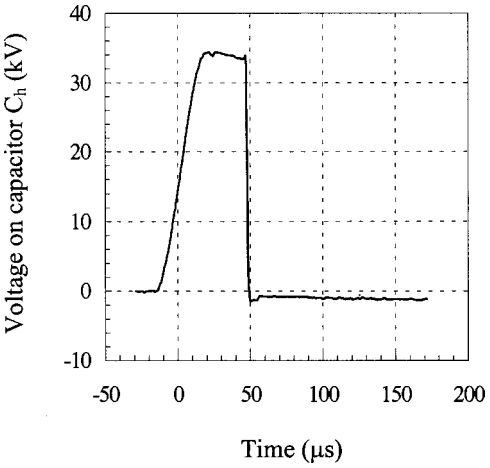

FIG. 4. Time-resolved voltage wave form on the high-voltage capacitor, C_h.

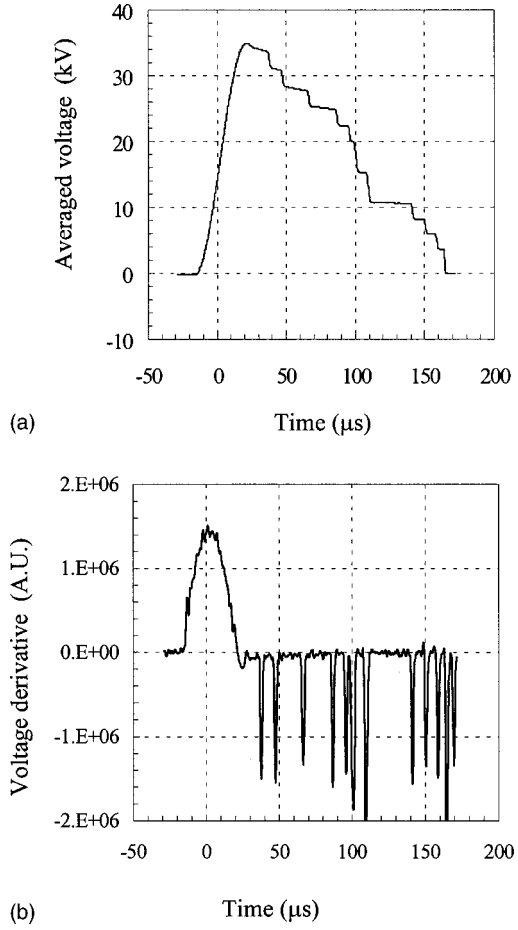

FIG. 5. (a) Time-resolved voltage wave form on the high-voltage capacitor, C_h. (b) Derivatives of the averaged voltage in (a).

correspond to the switching. Each negative peak corresponds to the fast voltage drop in Fig. 5(a) at the moment when the main spark gap is fired. In these examples, it can also be seen that the spark-gap switch always breaks down after the resonant charging process. With the time derivative of a large number of time-resolved voltage wave forms, the time delay for the spark-gap switching can be evaluated. By sampling 1000–4000 signals, Fig. 6 shows the time-resolved derivatives of the averaged voltage wave forms for pulse repetition

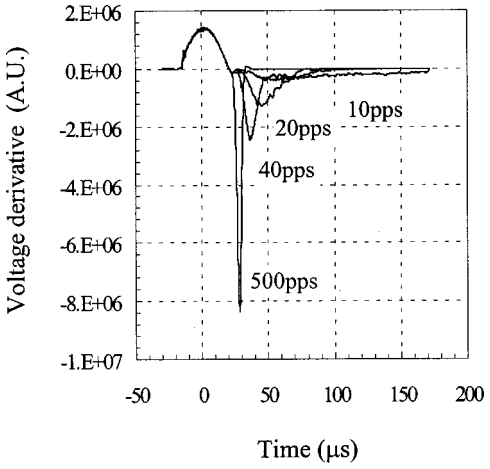

FIG. 6. Time delay distribution of the spark-gap switch.

rates of 10, 20, 40, and 500 pps, respectively. By increasing the pulse repetition rate, the distribution functions move to earlier times and their half widths decrease. According to our experimental observations, by optimizing the electrode geometry, the flush gas flow rate, and the time coefficient β, very stable spark-gap switching can be achieved.

B. Output characteristics of the generator

For corona plasma generation, wire–wire, wire–cylinder, and wire–plate reactors are under investigation for various corona-induced plasma applications, such as biogas cleaning and VOC emission abatement.[2,5,7] For example, using a wire–cylinder reactor with length and inner and outer diameters of 3000, 3, and 160 mm, respectively, a 2.0 kW averaged corona plasma can be generated with corona energy of 2.3 J/pulse at a pulse repetition rate of 860 pps.[6] With regard to the energy transfer for primary streamer propagation and matching between the generator and corona reactors,[4,5] a wire–plate corona reactor is used to match the present generator. Successive development of the present system is a 10–30 kW corona plasma system with a hybrid pulsed power source, which consists of a high-voltage pulse generator, as shown in Fig. 1, and a resonant capacitive charging unit. Sixteen wire–cylinder reactors in parallel with a total corona wire of 16 m are used to match the source.[8]

Figure 7 shows typical voltage and current output wave forms with a resistor load. The voltage rise time is about 20 ns, while the pulse duration depends on the time constant of $Z_{\text{in}}C_h$. As a function of the pulse repetition rate, Fig. 8 shows the typical averaged output power for three different energies per pulse. During these tests, the load resistor varied between 48 and 60 Ω because of the heating and the electric field. Both the pulse repetition rate f and the energy ϵ_p per pulse determine the average power $P=f\epsilon_p$. Figure 9 shows the standard deviation of the measured power in terms of the pulse repetition rate. After optimizing the spark-gap switch and its triggering circuit, the deviation is around 1.0% within the pulse repetition rate from 1 to 900 pps. Moreover, the high-voltage pulse generator could also maintain very stable outputs even if the main spark-gap switch is prefired.[9]

Previous investigations have indicated that the energy consumption contributes largely to the operating costs for industrial applications of pulsed corona techniques. The energy cost depends on both chemical reactions and the energy conversion efficiency from the main power line to the plasma reactor. The energy conversion efficiency of the system has been investigated for each step of the circuit. The total energy conversion efficiency from the main power line to a corona reactor can be divided into two subefficiencies. The first one η_1 is for charging high-voltage capacitor C_h, while the second, η_2, is the efficiency of transferring the stored energy in C_h to the corona reactor. For the first one, the main losses are because of the thyristor snubber and the pulse transformer. The energy conversion efficiency of the present pulse transformer is around 98%, while the losses on snubbers mainly depend on the capacitance ratio of the snubber capacitor over low-voltage capacitor C_L. As shown in Fig. 1, three air coil inductors are used for resonant charging

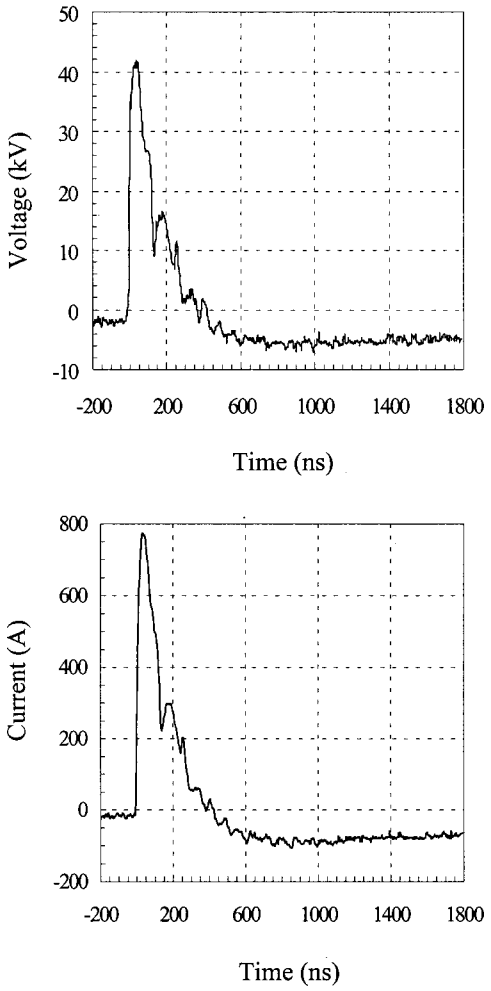

FIG. 7. Typical voltage and current output wave forms with a resistor load.

and/or discharging process.[6] Subefficiency η_1 increases with increasing energy per pulse. For an energy output of around 10 J/pulse, η_1 is around 95%.

For the second subefficiency, η_2, the triggered spark-gap switch, the transmission line transformer, and the matching between the generator and the reactor mainly cause the losses. We found that, for each corona reactor, there is a

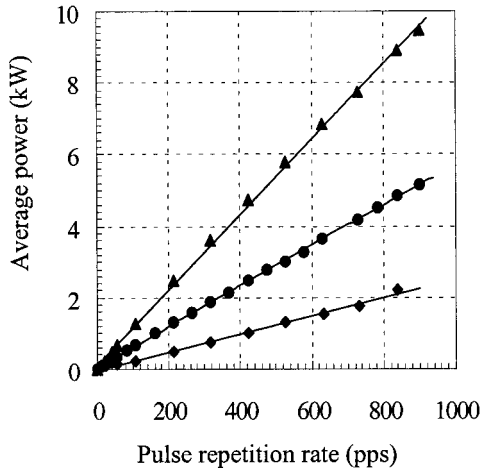

FIG. 8. Typical output of average power in terms of the pulse repetition rate and the energy per pulse: (■) 2.2–2.6; (●) 5.7–6.3; (▲) 10.5–12.0 J/pulse.

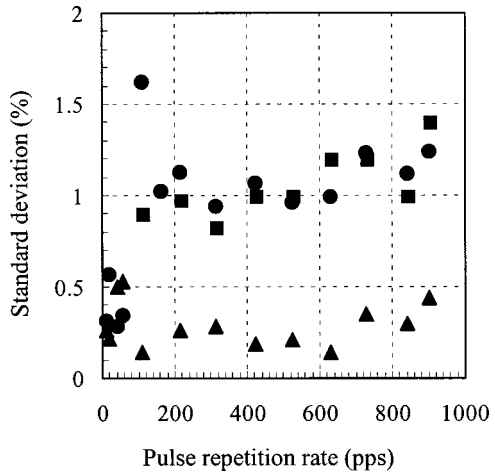

FIG. 9. Typical standard deviation in terms of the pulse repetition rate under various energies per pulse: (■) 5.6–6.3; (●) 8.8–9.8; (▲) 10.5–12.0 J/pulse.

minimum peak voltage required for achieving the maximum energy transfer from the pulse generator to the corona reactor. By increasing the peak voltage beyond the minimum voltage, the equivalent impedance of the corona reactor, R_{reactor}, defined as the ratio of the peak voltage over the peak current, approaches the output impedance of the generator. Subenergy conversion efficiency η_2 can be generally approximated by

$$\frac{\eta_2}{\eta_{2-\max}} = \frac{4\theta}{(1+\theta)^2},$$

where $\theta = R_{\text{reactor}}/Z_{\text{out}}$.[5] The resistor ratio θ mainly depends on the peak voltage, while the maximum energy transfer efficiency $\eta_{2-\max}$ mainly depends on the TLT design. When the TLT, constructed with a ring core ferrite, is connected in series at the output side ($Z_{\text{out}} = 200\,\Omega$), $\eta_{2-\max}$ is about 80%.[5] This lower energy conversion efficiency is caused by ferrite saturation. For the present design, larger size microgapped Metglas cores are used to prevent saturation and to increase the secondary mode impedance,[6] which gives $\eta_{2-\max}$ of around 96%. When the peak voltage on the reactor becomes larger than the minimum voltage, we have $\theta = R_{\text{reactor}}/Z_{\text{out}} \approx 1$, and the efficiency η_2 approaches the maximum energy transfer efficiency, $\eta_{2-\max}$, which is obtained with a matched resistor as the load. As a result, the total energy efficiency $\eta = \eta_1 \eta_2$ for the present system is of the order of 80%–90%.

Moreover, the generator has been tested for more than 100 h for both industrial demonstrations, such as testing on styrene and odor removal from air,[7] and laboratory investigations at an average output power of 1–10 kW. The electrodes are slightly eroded; detailed discussions on the reliability, lifetime, and industrial testing on VOC removal, odor control, and biogas cleaning will be reported in separate papers.

IV. DISCUSSION

An energy efficient repetitive high-voltage pulse generator has been developed for both laboratory investigation and industrial applications. The following features have been obtained.

(1) A three-step resonant charging circuit can automatically adapt to a triggered spark-gap switch and a TLT for generating nanosecond high-voltage pulses. The pulse to pulse deviation of the output pulsed energy can be controlled to be less than 1.0% for a pulse repetition rate of 1–900 pps. The system has been tested for more than 100 h without any trouble.
(2) According to achieved results, a pulsed power source with average power of up to 30 kW is also under investigation with a matched corona reactor. Detailed results will be reported in the near future.

ACKNOWLEDGMENT

The authors thank the European Commission for supporting this work.

[1] *Electrical Discharges for Environmental Purposes: Fundamentals and Applications*, edited by E. M. van Veldhuizen (Nova Science, New York, 2000).
[2] E. J. M. van Heesch, A. J. M. Pemen, K. Yan, P. P. M. Blom, A. H. J. Huijbrechts, and P. C. T. van der Laan, J. Tech. Phys. **41**, 273 (2000).
[3] K. Yan, H. Hui, M. Cui, J. Miao, X. Wu, C. Bao, and R. Li, J. Electrost. **44**, 17 (1998).
[4] K. Yan, E. J. M. van Heesch, E. M. van Veldhuizen, M. Rea, and R. Li, J. Adv. Oxid. Technol. **4**, 312 (1999).
[5] K. Yan, E. J. M. van Heesch, A. J. M. Pemen, and P. A. H. J. Huijbrechts, Plasma Chem. Plasma Process. **21**, 107 (2001).
[6] K. Yan, E. J. M. van Heesch, A. J. M. Pemen, P. A. H. J. Huijbrechts. F. M. van Gompel, Z. Matyas, and H. van Leuken, 35th IEEE–IAS Annual Meeting, Rome, Italy, 8–12 October 2000, pp. 592–599.
[7] K. Yan, E. J. M. van Heesch, A. J. M. Pemen, and P. A. H. J. Huijbrechts, J. Electrost. (in press).
[8] K. Yan, F. M. van Gompel, E. J. M. van Heesch, and A. J. M. Pemen, Third International Symposium on Nonthermal Plasma Technology for Pollution Control, 23–27 April 2001, Korea.
[9] K. Yan, E. J. M. van Heesch, A. J. M. Pemen, and P. C. T. van der Laan (unpublished).